Materials Advances

ROYAL SOCIETY OF CHEMISTRY

PAPER

View Article Online
View Journal | View Issue

Cite this: *Mater. Adv.*, 2023, 4, 2127

Bis-quaternary ammonium betulin-based dimethacrylate: synthesis, characterization, and application in dental restorative resins†

Lusi Zhang,‡ Zhiyuan Ma,‡ Ruili Wang,* Weiwei Zuo and Meifang Zhu

Secondary caries is the most common reason for restoration failures in general dental practices, resulting from tooth-adherent cariogenic bacteria in the oral environment. The application of polymerizable quaternary ammonium monomers (QAMs), which are capable of copolymerizing with methacrylate monomers and immobilizing antimicrobials in dental materials simultaneously, is expected to be an attractive anticaries strategy. In this work, three types of bis-quaternary ammonium betulin-based dimethacrylate derivatives (Bis-QADM-Bet) were synthesized *via* a Menschutkin reaction. Their chemical structures mainly differ for alkyl chain lengths of 4, 8, and 12 carbons (namely C4, C8, and C12). We focused on the fabrication of dental resins with 10 wt% Bis-QADM-Bet and a conventional dimethacrylate-based resin (bisphenol A glycerolate dimethacrylate/tri(ethyleneglycol) dimethacrylate, Bis-GMA/TEGDMA). The relationship between the Bis-QADM-Bet structure and the antibacterial activity, physicochemical properties, and cytotoxicity of dental resins were systematically investigated. The results indicated that regulating the alkyl chain length of Bis-QADM-Bet to C8 led to the formulated resin with superior effectiveness in terms of *S. mutans* inhibition ($p < 0.05$). Interestingly, this optimal resin exhibited better flowability and lower cytotoxicity in comparison with the Bis-GMA/TEGDMA based resin without compromising the mechanical properties ($p > 0.05$). Additionally, the potential antibacterial mechanism of contact-killing was proposed to illustrate the structural–morphological changes of *S. mutans*. In summary, this work shows that dental restorative resins containing Bis-QADM-Bet with the appropriate alkyl chain length are beneficial toward inhibiting the growth of *S. mutans* without sacrificing physicochemical performance.

Received 10th January 2023,
Accepted 27th March 2023

DOI: 10.1039/d3ma00016h

rsc.li/materials-advances

1. Introduction

Dental caries is one of the most prevalent oral diseases, affecting approximately 2.4 billion people worldwide.[1,2] The mechanism of dental caries is a carbohydrate diet-induced bacterial infectious disease, resulting from tooth-adherent cariogenic bacteria, primarily *Streptococcus mutans* (*S. mutans*) that converts sugars into organic acids inside plaque, leading to the demineralization and destruction of tooth over time.[3] Resin-based composites have been applied for restoring decayed teeth since the 1960s,[4,5] which are bonded in cavities *via* adhesives and photo-polymerized to form cross-linked networks. However, these composites accumulate more plaque than other materials, which elevates the bacterial proliferation of restorative surfaces and results in secondary caries and restoration failures.[6,7] Therefore, it is highly desirable to develop dental composites possessing superior antibacterial activity.

Attempts to incorporate soluble antibacterial compounds, such as silver and chlorhexidine, are considered as the feasible approach.[8,9] However, an initial burst release yielded short-term antibacterial activity and compromised physical–mechanical properties.[10] Therefore, Imazato *et al.* proposed quaternary ammonium monomers (QAMs), which are capable of copolymerizing with conventional methacrylate monomers, leading to the formation of polymer networks and the immobilization of antimicrobials in dental materials simultaneously.[11–13] The number of methacrylate groups and quaternary ammonium functionalities affects the performance of materials.[14–17] Monomethacrylate QAMs demonstrated remarkable antibacterial

State Key Laboratory for Modification of Chemical Fibers and Polymer Materials, College of Materials Science and Engineering, Donghua University, Shanghai 201620, China. E-mail: wangruili@dhu.edu.cn

† Electronic supplementary information (ESI) available: Fig. S1–S3 show ^{1}H and ^{13}C NMR spectra, FT-IR spectra, and HRMS of betulin, betulin-based bromide intermediates (DEB-Bet, DBB-Bet, and DHB-Bet) and Bis-QADM-Bet (EBet, BBet, and HBet). Fig. S4 (PDF) shows the primer sequences used for RT-qPCR analysis, the amplification and melting curves, the gel electrophoresis image, and RNA concentration and OD_{260}/OD_{280} ratio of *S. mutans* after coculture with 5B5T and 1BBet4B5T for 24 h. See DOI: https://doi.org/10.1039/d3ma00016h

‡ These authors contributed equally to this work.

effects, but these monomers could only undergo linear polymerization, which ultimately adversely affected physicochemical properties of materials once beyond their maximum addition (~5 wt%).[18,19] In contrast, di-methacrylate QAMs led to higher addition (10–60 wt%) in resins, but the antibacterial activity depended on the monomer concentration.[20,21] A remedy for these issues is the design of bis-quaternary ammonium dimethacrylate (bis-QADM) to maintain a balance between mechanical properties and antibacterial effects. However, only a few examples are found in the published work.[20,22–24] Fanfoni *et al.* developed nine different types of antibacterial bis-QADM, considering the spacer and geometry of quaternary ammonium functionalities, the ionic counterions, *etc.*[20] All these monomers inhibited *S. mutans* biofilm formation at a concentration equal to the minimum inhibitory concentration (MIC), showing potential applications in dentistry.

Inspired by these studies, the advantageous structural characteristics of bis-QADM could be adopted to optimize the chemical structure of betulin, which has not been reported. As an abundant naturally occurring triterpene wildly distributed in plants, betulin possesses excellent anticancer and antimicrobial activities.[25,26] Our previous work found that dimethacrylate-functionalized betulin derivatives (M_2Bet) made the resultant resin exhibit significantly higher inhibitory effects against *S. mutans* than control, but the inhibition rate was only 83.1%.[27] Herein, we designed three types of bis-quaternary ammonium betulin-based dimethacrylate derivatives (Bis-QADM-Bet) *via* the Menschutkin reaction. Their chemical structures mainly differ for alkyl chain lengths of 4, 8, and 12 carbons. It is speculated that Bis-QADM-Bet-containing dental resins would be able to achieve a stronger antibacterial effect without sacrificing the mechanical properties by combining the inherent antibacterial activity of betulin and the favorable structural features of bis-QADM. The objective of this work is to investigate the effect of the chemical structure of Bis-QADM-Bet on the physicochemical properties, polymerization kinetics, cytotoxicity, and antibacterial activity, while searching for a clear structure–property relationship of the formulated dental resins.

2. Materials and methods

2.1. Materials

Betulin (≥98%) was received from Tianjin NWS Biotechnology and Medicine Co., Ltd (Tianjin, China). Triethylamine (TEA, ≥99%), 6-bromohexanoyl chloride, 4-bromobutyryl chloride, and bromoacetyl chloride were purchased from Aladdin (Shanghai, China). Dimethylaminoethyl methacrylate (DMAEMA, 99%), bisphenol A glycerolate dimethacrylate (Bis-GMA, >98%), tri(ethyleneglycol)dimethacrylate (TEGDMA, 95%), ethyl-4-dimethylaminobenzoate (4-EDMAB, 99%), and camphorquinone (CQ, 97%) were purchased from Sigma-Aldrich (Shanghai, China). *Streptococcus mutans* (*S. mutans*, ATCC 25175) was provided by Mingzhou Biological Technology Co., Ltd (Ningbo, China). Human dental pulp cells ($HDPC_S$) were purchased from Guangzhou Saiku Biotechnology Co., Ltd (Guangzhou, China).

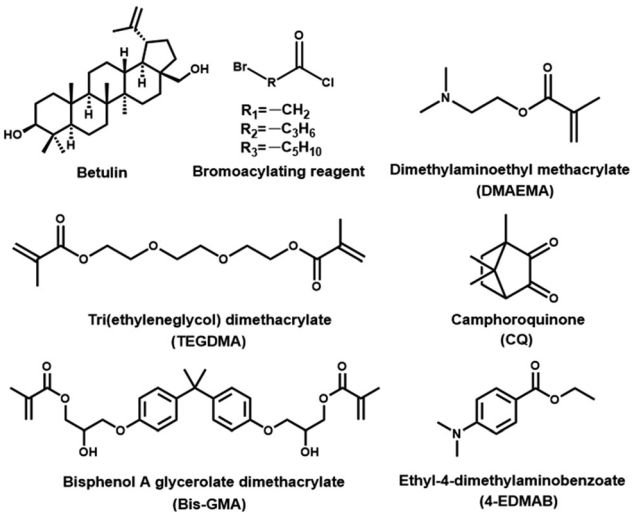

Fig. 1 Chemical structures of the representative materials used in this study.

The chemical structures of the representative materials are illustrated in Fig. 1.

2.2. Synthesis of Bis-QADM-Bet

Bis-QADM-Bet was synthesized through the quaternization of a trialkylamine (Scheme 1), known as the Menschutkin reaction. Briefly, three types of betulin-based bromide intermediates were firstly synthesized with different bromoacylating agents, including di(ethyl ester bromide)betulin-based derivative (DEB-Bet), di(butyl ester bromide)betulin-based derivative (DBB-Bet), and di(hexyl ester bromide)betulin-based derivative (DHB-Bet). Afterwards, the quaternization reactions of each bromide intermediate and a methacrylate-containing tertiary amine (DMAEMA) were performed. The obtained products were noted

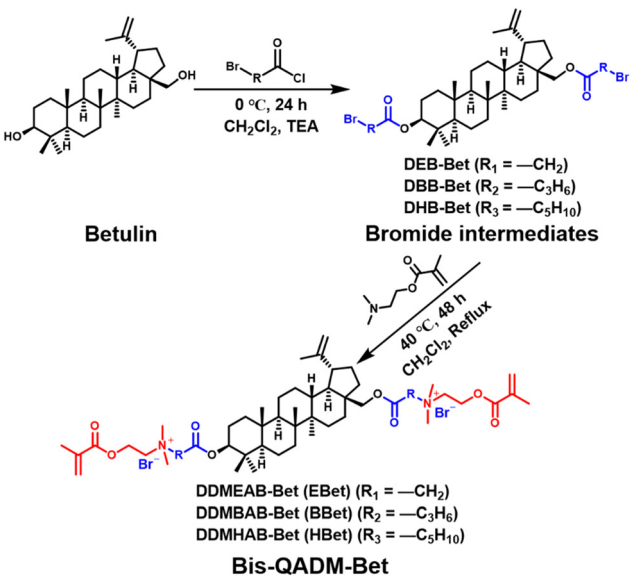

Scheme 1 Synthetic route of Bis-QADM-Bet by a two-step Menschutkin reaction using betulin as the starting material.

Table 1 Three types of Bis-QADM-Bet with various alkyl chain lengths

Betulin-based bromide intermediate	Tertiary amine	Product (Bis-QADM-Bet)	Alkyl chain length of product[a]
DEB-Bet	Dimethylaminoethyl methacrylate (DMAEMA)	DDMEAB-Bet (EBet)	4
DBB-Bet		DDMBAB-Bet (BBet)	8
DHB-Bet		DDMHAB-Bet (HBet)	12

[a] The betulin backbone is not included.

as di(dimethylaminoethyl methacrylate ethylammonium bromide)-betulin-based derivative (DDMEAB-Bet), di(dimethylaminoethyl methacrylate butylammonium bromide)betulin-based derivative (DDMBAB-Bet), and di(dimethylaminoethyl methacrylate hexylammonium bromide)betulin-based derivative (DDMHAB-Bet), which were further abbreviated as EBet, BBet, and HBet, respectively (Table 1).

2.2.1. Synthesis of EBet. Betulin (4.0 g, 9.0 mmol), TEA (2.5 mL, 18.1 mmol), and dichloromethane (70.0 mL) were added into a 250 mL round-bottom flask and the solution was magnetically stirred for 15 min. 2-Bromoacetyl chloride (2.2 mL, 26.4 mmol) dissolved in 40.0 mL dichloromethane was then added dropwise into the above solution. After reacting at 0 °C for 24 h, the obtained mixture was washed three times with 5% aqueous NaOH and deionized water, and dried with anhydrous $MgSO_4$. The organic layer was purified by silica-gel column chromatography (ethyl acetate/petroleum ether = 1/12, v/v, as eluent) to obtain DEB-Bet as a white solid (3.5 g, 57.2% yield). Subsequently, for the quaternization reaction, DEB-Bet (1.0 g, 1.5 mmol) and DMAEMA (0.5 mL, 3.3 mmol) were dissolved in 10 mL of dichloromethane and placed in a 50 mL round-bottom flask under magnetic stirring and refluxed at 40 °C for 48 h. Once the reaction was completed, the solution was precipitated into diethyl ether and the solvent was removed by a rotary evaporator. The final EBet was obtained as a white powder (1.2 g, 79.1% yield; Fig. 2(C)). The structural details of DEB-Bet and EBet were confirmed using a high-field NMR spectrometer (AVANCE III HDTM, Bruker, Switzerland, ^{1}H NMR: 600 MHz, ^{13}C NMR: 151 MHz), a FT-IR spectrometer (Nicolet 8700, Germany) equipped with an ATR mode, and a high-resolution mass spectrometer (FT-ICRMS, Bruker Daltonics, USA), respectively. All the detailed results and analysis of DEB-Bet and EBet are presented in the ESI,† Fig. S1.

2.2.2. Synthesis of BBet and HBet. Similarly, during the synthesis procedure, BBet and HBet were synthesized by using 4-bromobutyryl chloride and 6-bromohexanoyl chloride as the bromoacylating reagent, respectively (Scheme 1), affording BBet as colorless viscous liquid (1.1 g, 80.3% yield; Fig. 2(C)) and HBet as low-viscosity liquid (0.9 g, 64.9% yield; Fig. 2(C)). Their chemical structures are also confirmed in Fig. S2 and S3 (ESI†).

2.3. Fabrication of dental resins

To prepare neat dental resins, the as-synthesized Bis-QADM-Bet monomers, including EBet, BBet, and HBet, were incorporated at 10 wt% into the Bis-GMA/TEGDMA based resin according to our previous work.[27] The corresponding resin formulations were denoted as 1EBet4B5T, 1BBet4B5T, and 1HBet4B5T, respectively. Commercial resins including 50 wt% Bis-GMA and 50 wt% TEGDMA (5B5T) served as the control group.[28] During the fabrication process, both monomers and photo-initiators (CQ and 4-EDMAB, 0.2/0.8, wt/wt) were mixed using a Speed Mixer (DAC 150.1 FVZ-K, Germany) at 2000 rad s^{-1} for 3 min and the obtained resin paste was put in a vacuum oven to remove air bubbles. A polymerization process was then performed using a light unit (SLC-8D, 430–490 nm, 800–1200 mW cm^{-2}, Hangzhou Sifang Medical Instrument Co., China) to prepare resin samples for 60 s on each side.

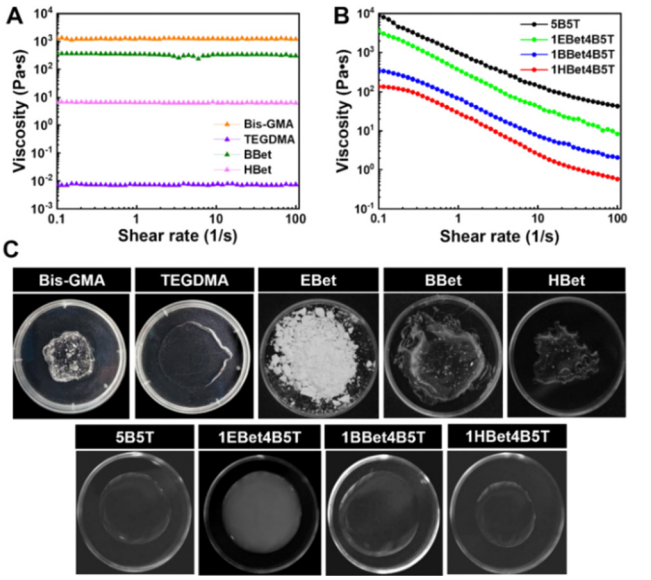

Fig. 2 Shear viscosity of Bis-GMA, TEGDMA, BBet, and HBet (A) and the formulated 5B5T, 1EBet4B5T, 1BBet4B5T, and 1HBet4B5T resins (B), digital photos of these monomers and resin formulations (C).

2.4. Viscosity

The rheological behavior was evaluated using a rotational rheometer (Modular Compact Rheometer 302, Anton Paar, Austria). Each resin sample (0.5 mL) was put on the parallel plate (25 mm). Steady shear sweep measurements were carried out at shear rates of 0.1 to 100 s^{-1} to determine the shear viscosity at 37.0 ± 0.5 °C.

2.5. Light transmittance and refractive index

Light transmittance of each cured resin sample (Φ 10 mm × 1 mm) from 200 to 480 nm was measured using a UV-vis-NIR spectrophotometer (UV3600, Shimadzu, Japan). Additionally, the refractive index (RI) of dental resins without photo-initiators was recorded on an Abbe-type refractometer (DR-M2, Japan) (n = 5).

2.6. Real-time degree of conversion

Real-time observation of the photo-polymerization process of dental resins was carried out using a FT-IR spectrophotometer (Nicolet 8700, Germany) with an ATR accessory. Each unpolymerized resin sample (5 μL, $n = 3$) was carefully put on an ATR crystal, covered with a glass slide, and the corresponding FTIR spectrum before polymerization was measured. Subsequently, the resin sample was photo-polymerized and the real-time FTIR spectrum was recorded every 10 s until 10 min. Based on each spectrum, the heights of the absorption peaks of aliphatic C=C band (1638 cm^{-1}) and the aromatic C=C band (1608 cm^{-1}) were measured, respectively. The degree of conversion of dental resins at each polymerization time was calculated using eqn (1):[29,30]

$$\text{Degree of conversion}\,(\%) = \left(1 - \frac{(h_{1638}/h_{1608})_{\text{cured}}}{(h_{1638}/h_{1608})_{\text{uncured}}}\right) \times 100\% \quad (1)$$

where $(h_{1638}/h_{1608})_{\text{uncured}}$ and $(h_{1638}/h_{1608})_{\text{cured}}$ indicate the peak height ratio at 1638 to 1608 cm^{-1} before and after curing, respectively.

2.7. Mechanical properties

The flexural and compressive properties of dental resins were measured using a universal testing machine (Instron 33R 4201, USA). Rectangular-shaped bars (25 mm × 2 mm × 2 mm, $n = 6$) and cylindrical specimens (Φ 4 mm × 6 mm, $n = 6$) were made from each resin formulation and applied to the three-point bending tests (span of 20 mm and crosshead speed of 0.75 mm min^{-1}) and the compressive tests (loading rate of 0.75 mm min^{-1}), respectively, as described in our previous work.[27]

2.8. *In vitro* cell viability

Resin discs (Φ 10 mm × 1 mm, $n = 6$) were made from each resin and co-incubated with culture medium at 37 °C for 24 h to produce the extraction solution, according to ISO 10993-5.[31] The detailed procedure was based on our previous work.[27] In brief, each solution was diluted with fresh culture medium to 1 : 1 (v/v), transferred to the 96-well plates at a density of 1×10^3 HDPCs per well, and cultured for 1, 3, 5, and 7 days, respectively. After each culture point, the cell viability was determined using CCK-8 assay. The obtained optical density (OD) was recorded at a wavelength of 450 nm on a microplate reader (Elx800, USA). Furthermore, HDPCs were stained with Calcein-AM/PI kit for 15 min, and the cell morphology of dental resins was investigated using a fluorescence microscope (Leica DMi8, Germany).

2.9. Water contact angle

Ultra-pure water (2 μL) was injected on the surface of the resin sample (Φ 15 mm × 1 mm, $n = 5$) *via* a micro-syringe. The water contact angle of dental resins was determined using a contact angle meter (OCA 20, Dataphysics, Germany), which was calculated by the slope of the tangent to the liquid drop at the liquid–solid–vapor interface line.

2.10. *In vitro* antibacterial activity

2.10.1. Bacteria culture. *S. mutans* was selected as the bacterial model to evaluate the antibacterial activity of dental resins in this work. *S. mutans* was cultured in a brain heart infusion (BHI) broth under an anaerobic atmosphere (90% N_2, 5% CO_2, and 5% H_2) at 37 °C for 18 h.[32] The bacteria were grown overnight, collected by centrifugation, and washed three times with PBS. The concentration of the bacterial suspension was diluted to 1×10^6 colony-forming units (CFU) mL^{-1}.

2.10.2. Plate-counting method. Resin samples (Φ 15 mm × 1 mm, $n = 3$) were co-incubated with the bacterial suspension (80 μL) at 37 °C for 24 h. The samples were then transferred to the centrifuge tube containing 8 mL of sterile normal saline and sonicated for 5 min. The obtained bacterial suspension was serially diluted with PBS and spread uniformly onto BHI agar plates. After 48 h of culture, the bacterial colonies were counted and the CFU counts were determined.

2.10.3. Bacterial morphology of bacterial cells. Similarly, resin specimens (Φ 15 mm × 1 mm, $n = 3$) were further made and co-incubated with bacterial suspension at 37 °C for 24 h. The bacterial solution at OD = 0.5–0.8 was collected by centrifugation and divided equally into three parts. (1) One part (1 mL) was dually stained using a LIVE/DEAD BacLight bacterial viability kit (SYTO9-PI) at 37 °C for 15 min. The live–dead status of bacteria on each sample was visualized using a confocal laser scanning microscope (CLSM, Olympus FV1200, Japan). (2) Another part of the bacterial solution (1 mL) was fixed with glutaraldehyde (2.5% in H_2O) for 24 h, dehydrated with a series of ethanol solutions (30, 50, 70, 80, 90, 95, and 100%) for 15 min each, and supercritically dried. The bacterial morphology of each material was observed on a field emission scanning electron microscope (FE-SEM, SU8010, Japan). (3) The rest of the bacterial solution (1 mL) was dehydrated and supercritically dried as mentioned above. The bacteria were embedded in Epon/Araldite resin at 70 °C overnight. Ultrathin sections (70–90 nm) were stained with 4% uranyl acetate and 0.2% lead citrate for 5–10 min. The bacterial morphology was further evaluated using a transmission electron microscope (TEM, Talos F200S, USA).[33]

2.11. Bacterial growth kinetic tests

The antibacterial effectiveness of dental resins was further assessed within 48 h according to the bacterial growth kinetic study. That is, the *S. mutans* outgrowth was monitored by determining the absorbance value at a wavelength of 600 nm (OD_{600}). Each resin disc (Φ 15 mm × 1 mm, $n = 3$) was co-incubated with bacterial suspension (0.5 mL) at 3, 6, 9, 12, 24, and 48 h, respectively. At each time interval, 100 μL of each solution was transferred into the 96-well plates and the OD_{600} value was recorded on a microplate reader (Elx800, USA).

2.12. Protein leakage and ion-release analysis

Quantitative analysis of protein leakage from bacteria was performed as previously reported.[34] In general, resin samples (Φ 15 mm × 1 mm, $n = 3$) were placed into the centrifugation

tubes containing 10 mL bacterial suspension. After incubating in an anaerobic atmosphere at 37 °C for 24 h, 500 μL lysis solution was added into each tube, and the obtained mixture was cultured on an orbital shaker at 37 °C for another 30 min. Afterwards, the bacterial cells of each sample were collected by centrifugation and washing with PBS twice. The total protein concentration was detected *via* a BCA protein assay kit (BCA02, China) using a microplate reader at λ = 562 nm. Meanwhile, the supernatant after centrifugation was selected to determine the ion release of K^+, Fe^{3+}, and Mg^{2+} by inductively coupled plasma optical emission spectrometry (ICP-OES, Aglient 5110, USA).

2.13. Real-time quantitative polymerized chain reaction (RT-qPCR) assay

Glucosyltransferases (gtfs) is responsible for the synthesis of extracellular glucans from *S. mutans*, which promotes the bacterial adhesion to human teeth. Gtfs expression in *S. mutans* involves glucosyltransferase B (*gtfB*), glucosyltransferase C (*gtfC*), and glucosyltransferase D (*gtfD*). Thus, the transcription levels of *gtfB*, *gtfC*, and *gtfD* were evaluated by RT-qPCR.[35] Briefly, resin discs (Φ 15 mm × 1 mm, n = 3) were put into the *S. mutans* suspension (10 mL) and cultured at 37 °C for 24 h, as described above. The cultures were centrifuged, rinsed with PBS twice, and *S. mutans* attached onto the surface of resin samples was harvested for RNA extraction. For the further analysis of complementary DNA (cDNA), RNA was reverse-transcribed using a RT Master Mix kit (FSQ-201, Toyobo, Japan). The obtained cDNA (1 μL) was applied as a template for RT-qPCR amplification, which was performed at 95 °C for 2 min followed by 45 cycles at 95 °C for 15 s, 60 °C for 20 s, and 72 °C for 20 s, respectively. RT-qPCR was performed to determine gene expression in a LightCycler 480 Real-Time PCR System (Roche, USA). All primer sequences for RT-qPCR and their amplification curves and melting curves are collected and shown in Fig. S4(A)–(C) (ESI†). The gene expression was normalized to 16S rRNA of *S. mutans*. Three separate tests were performed for each dental resin. The purity of DNA and the OD_{260}/OD_{280} ratio of RNA extractions were determined by agarose gel electrophoresis (PowerPac basic, Bio-Rad, USA) and Nanodrop Microvolume UV-Vis spectrophotometry (2000/2000c, Thermo Fisher Scientific, USA), respectively, and the results are exhibited in Fig. S4(D) and (E) (ESI†).

2.14. Statistical analysis

One-way analysis of variance (ANOVA) and Tukey's multiple comparison test were carried out in this study using SPSS software (version 20.0, IBM Corp., USA) with a significance level set at $p < 0.05$.

3. Results and discussion

3.1. Structure validation

In this work, Bis-QADM-Bet were synthesized *via* a two-step Menschutkin reaction (Scheme 1). Their structures are confirmed by ^{1}H and ^{13}C NMR spectra, FT-IR spectra, and HRMS (Fig. S1–S3, ESI†).

3.2. Viscosity

Viscosity is a predominant factor determining the design of a monomer structure and the formulation of resin mixtures. In general, a low monomer viscosity does not affect its miscibility with resin matrix, leading to higher filler loading, increased physical–mechanical properties, and improved processability of dental composites.[23] The shear viscosity of BBet and HBet was initially identified, and the results are compared with Bis-GMA and TEGDMA (Fig. 2(A) and (C)). All these monomers exhibit a Newtonian rheological behavior, *i.e.*, their viscosity remains constant as the shear rate increases (Fig. 2(A)). As expected, an extremely high viscosity is observed for Bis-GMA (1257.4 Pa s), due mainly to the strong intermolecular hydrogen bonding from hydroxyl groups in its bulky chemical structure. In contrast, TEGDMA possessing a linear molecular structure shows the lowest viscosity (0.008 Pa s). In terms of the synthesized monomers, BBet (359.3 Pa s) and HBet (6.68 Pa s) are more viscous than TEGDMA, but less so than Bis-GMA.

All these monomers were further physically mixed to formulate dental resins, where three experimental groups, 1EBet4B5T, 1BBet4B5T, and 1HBet4B5T, as well as the control group (5B5T), all display a non-Newtonian shear-thinning behavior (Fig. 2(B)).[36] The viscosity of 5B5T reaches a maximum value, followed by 1EBet4B5T, 1BBet4B5T, and 1HBet4B5T, as a result of a decrease of the intermolecular interactions, since the hydroxyl group is absent in EBet, BBet, and HBet, respectively. Furthermore, different alkane chain length of these synthesized monomers determines the viscosity of resins. With increasing the alkane chain length from 4, 8, to 12, the chain flexibility of EBet, BBet, and HBet is gradually increased, and can thereby accelerate the movement of monomer molecules.[37] That is, a longer alkane chain, especially for HBet, increases the distance between monomers in resins and reduces the intermolecular forces, and thus, the viscosity of dental resins is progressively decreased. These results confirm that the addition of 10 wt% EBet, BBet, and HBet offers the corresponding resin better flowability than 5B5T. Digital photos of dental resins further validate the excellent miscibility (Fig. 2(C)).

3.3. Light transmittance

Light transmittance through dental resins determines their appearance, photoactivatability, and polymerization kinetic behaviors. The transmittance spectra of dental resins as a function of wavelength are plotted in Fig. 3(A). Since CQ exhibits a maximum absorption at 468 nm,[38] the transmittance of 5B5T, 1EBet4B5T, 1BBet4B5T, and 1HBet4B5T at this wavelength is measured as 88%, 80%, 90%, and 91%, respectively, and only 1EBet4B5T is significantly lower than 5B5T. Digital photos of these resins after light-curing also confirm the above results (Fig. 3(B)).

The loss of light transmittance (T) occurs due to light scattering differences in the refractive index of polymer resins,

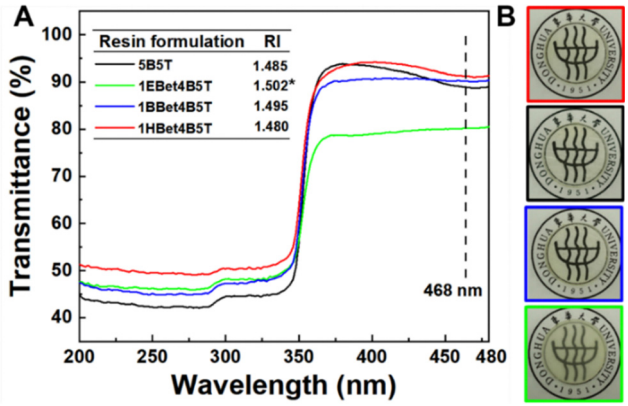

Fig. 3 Spectral transmittance curves and refractive index (inset image) of 5B5T, 1EBet4B5T, 1BBet4B5T, and 1HBet4B5T (A) and digital photos of their light-cured samples (size: Φ 15 mm × 1 mm) (B). *$p < 0.05$, compared with 5B5T.

showing an inverse relationship, as described in Rayleigh scattering (eqn (2)).[39] In this study, the refractive indexes of dental resins are listed in Fig. 3(A) (inset image), which follows the order 1EBet4B5T > 1BBet4B5T > 5B5T > 1HBet4B5T. This result further confirms that 1EBet4B5T has the lowest light transmittance, as a result of intensity attenuation of the transmitted light caused by the incorporated EBet (white-opaque powder, Fig. 2(C)). Conversely, the highest light transmittance is achieved for 1HBet4B5T.

$$T = \exp - 2303d\left[\frac{3V_p r^3\left(n_p/n_m - 1\right)}{4\lambda^4}\right] \quad (2)$$

where d is the thickness of the sample, V_p is the volume fraction of filler particles, r is the radius of particles, n_p is the refractive index of particles, n_m is the refractive index of the polymeric matrix, and λ is the light wavelength.

3.4. Polymerization behavior

During the photo-polymerization of multifunctional methacrylate-based dental materials, the monomer conversion is never complete.[40] The changes in the degree of double bond conversion of dental resins in real-time are shown in Fig. 4(A) and (B) to investigate their polymerization behavior. An increasing trend of degree of conversion of all resins within the first 2 min is found, and then tends to be balanced with the extension of curing time (Fig. 4(A)), as a result of a decrease in active free radicals. There is an obvious delay in the conversion kinetics for dental resins containing EBet and BBet, and the delay is prolonged with the decreasing of their alkane chain length. In contrast, 1HBet4B5T possessing HBet with the longest alkane chain length exhibits a similar polymerization behavior to 5B5T. These differences are attributed to weaker intermolecular hydroxyl bonding and lower viscosity of dental resins.[41,42] That is, with the partial replacement (10 wt%) of Bis-GMA by HBet in resin, the much less viscous 1HBet4B5T increases the mobility of monomers and contributes to a higher double-bond conversion compared with 1EBet4B5T and 1BBet4B5T.

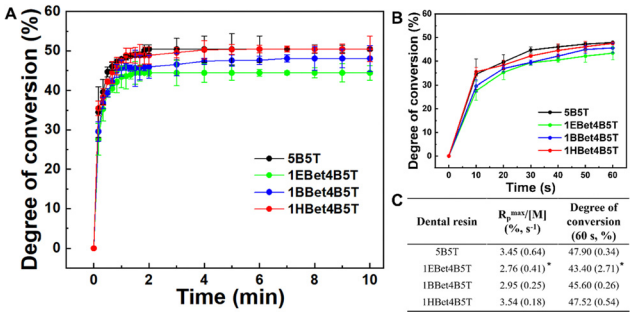

Fig. 4 Real-time conversion of C=C bonds of 5B5T, 1EBet4B5T, 1BBet4B5T, and 1HBet4B5T for 10 min (A) and 60 s (B) during the photo-polymerization process. R_p^{max}/[M] and degree of conversion (60 s) of these dental resins (C). R_p^{max}/[M]: the maximum slope of the linear region of degree of conversion *vs.* time plot.[27] *$p < 0.05$, compared with 5B5T.

Kinetics of polymerization for dental resins (Fig. 4(C)) further confirms the above results. In terms of the maximum polymerization rate (R_p^{max}/[M]) and degree of conversion (60 s), 1EBet4B5T exhibits significantly lower values than 5B5T whereas 1BBet4B5T and 1HBet4B5T present statistically similar values to the control. This is expected based on the similarity in the viscosity of these resins (Fig. 2(B)).

3.5. Mechanical properties

Superior mechanical properties are also essential to formulate dental resins. The mechanical properties of all investigated resins were evaluated for flexural strength, flexural modulus, and compressive strength (Fig. 5). The results of both flexural modulus and compressive strength show that there are no statistically significant differences between the resins assessed (Fig. 5(B) and (C)). However, in terms of flexural strength (Fig. 5(A)), the values of 1BBet4B5T and 1HBet4B5T are similar to the control 5B5T. Only 1EBet4B5T has a significantly lower flexural strength, likely due to the lowest R_p^{max}/[M] and the lowest conversion value observed in its polymerization kinetics (Fig. 4(C)). Since flexural strength is strongly associated with some important clinical assessments of dental materials, it is speculated that 10 wt% substitution of Bis-GMA by BBet or HBet could endow dental resins with adequate mechanical performance.

3.6. *In vitro* cell viability

The *in vitro* cell viability of dental resins as a function of culture time is displayed in Fig. 6(A). There is a progressive increase in OD of each material along with the increase in culture time, suggesting that the cell growth of all studied resins exhibits a continuous upward trend. All three experimental resins show no statistically significant difference in OD compared to 5B5T after 1 day of culture, which is also observed at the time point of 3 days except 1EBet4B5T. With the extension of the culture time to 5 and 7 days, the cell population in all experimental resins is greater than 5B5T ($p < 0.05$). These results suggest that 10 wt% addition of EBet, BBet, and HBet into resin mixtures does not influence the cell growth and proliferation.

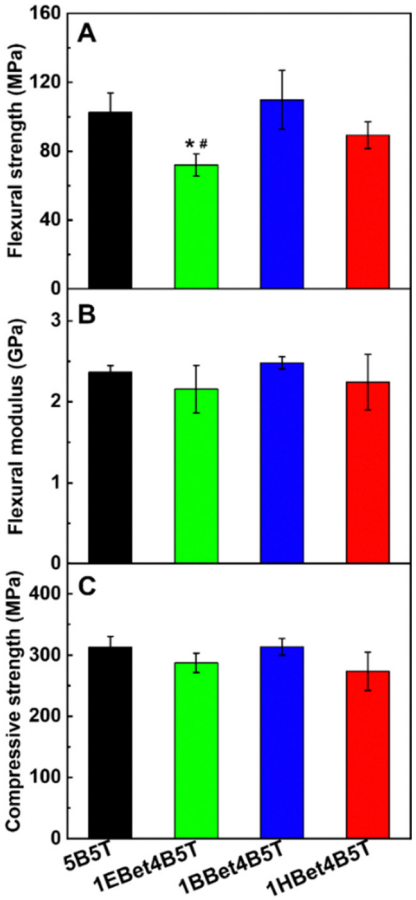

Fig. 5 Flexural strength (A), flexural modulus (B), and compressive strength (C) of 5B5T, 1EBet4B5T, 1BBet4B5T, and 1HBet4B5T. $^{*}p < 0.05$, compared with 5B5T. $^{\#}p < 0.05$, compared with 1BBet4B5T.

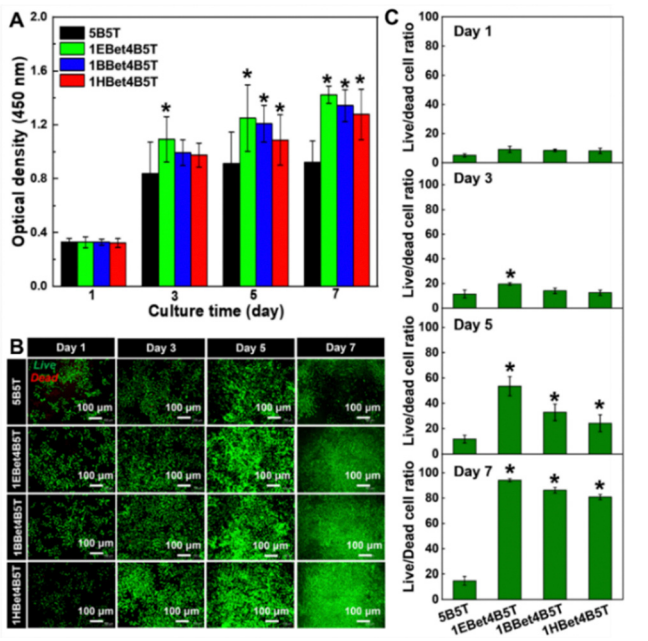

Fig. 6 CCK-8 assay of HDPCs viability cultured onto 5B5T, 1EBet4B5T, 1BBet4B5T, and 1HBet4B5T after 1, 3, 5, and 7 days of culturing (A). Fluorescence microscopy images of the morphology of HDPCs grown on these dental resins at each culture period, where green and red fluorescence indicates live and dead cells, respectively (B). Live/dead cell ratio of dental resins assessed from the fluorescent micrographs using ImageJ software (C). $^{*}p < 0.05$, compared with 5B5T.

An ideal dental resin for its application in hard-tissue repair should also provide an advantageous microenvironment for cell attachment, proliferation, and migration. The morphology of HDPCs grown on dental resins after different culture times was observed using a fluorescence microscope (Fig. 6(B)). As speculated, an increasing trend of live cells with spindle-like morphology is clearly found in all resins with the extension of culture time, especially for three experimental groups. These fluorescence images were further applied to quantitatively determine the live/dead cell ratio of each material (Fig. 6(C)). The addition of EBet, BBet, and HBet leads to the three experimental resins with higher live/dead cell ratio than 5B5T at each time interval, which confirms their better cell viability and agrees with the CCK-8 results (Fig. 6(A)).

3.7. Antibacterial activity

S. mutans is an anaerobic bacterium highly associated with the development of dental caries, due to its acidogenicity, aciduricity, and the ability to produce extracellular polysaccharides.[43] As observed from the survival colonies of *S. mutans* (small white dots) grown on each resin (Fig. 7(A)), the densest colonies are found on the control 5B5T, whereas no viable *S. mutans* are detected on 1EBet4B5T, 1BBet4B5T, and 1HBet4B5T. Quantitative results of the CFUs counts of *S. mutans* (Fig. 7(B)) exhibit that the bacterial concentration of these three experimental resins is zero, compared with that of 5B5T (8.7×10^8 CFU mL^{-1}), demonstrating that experimental resins have stronger antibacterial activity with a more than 99.9% antibacterial efficiency against *S. mutans*. In contrast, the inhibition rate of the $1M_2$Bet4B5T resin was only 83.1% in our previous study.[27] Therefore, the bis-quaternary ammonium groups of Bis-QADM-Bet are ideal for producing dental resins with superior antibacterial activity. The optical live/dead bacterial viability images in Fig. 7(C) demonstrate that a significantly higher number of live bacteria is detected on the surface of 5B5T and almost no live *S. mutans* existing on three experimental resins, further indicating that the antibacterial activity of dental resins is greatly increased by incorporating EBet, BBet, and HBet.

3.8. Bacterial growth kinetics

The antibacterial activity of dental resins is further studied by the bacterial growth kinetics and the results are plotted as changes in OD_{600} values with the culture duration (Fig. 7(D)). For 5B5T, the growth of *S. mutans* is in the exponential phase and continues until 24 h, and then enters directly into the decline phase. 1HBet4B5T exhibits a similar growth curve to 5B5T, but a better antibacterial activity is evident from the significantly lower OD value in the onset of the logarithmic growth phase. In contrast, stronger inhibition of bacterial growth is achieved by incorporating EBet and BBet into dental resins.

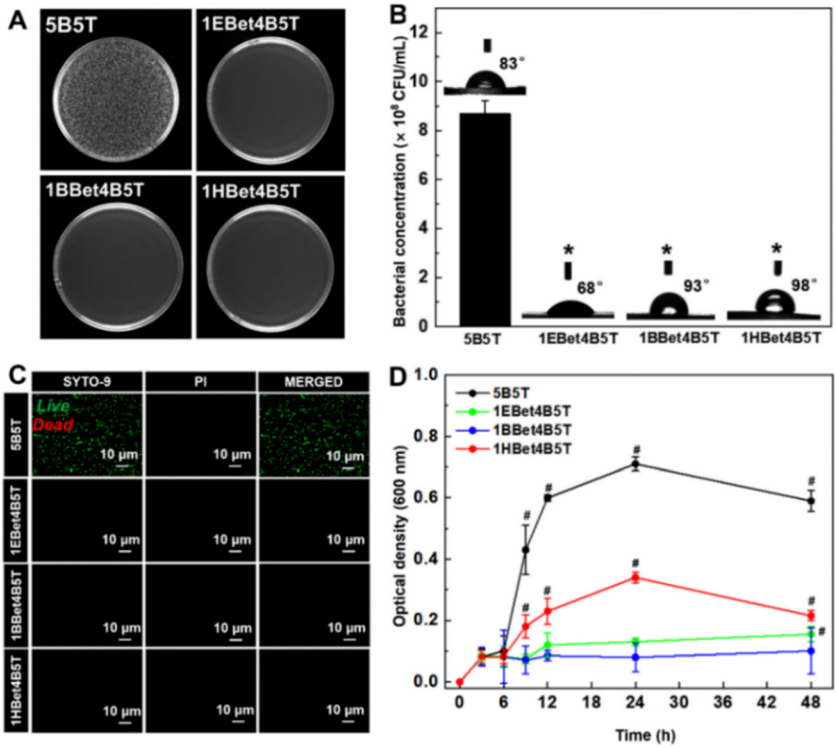

Fig. 7 Digital images of bacterial colonies (A) and the quantitative bacterial concentration (B) of *S. mutans* after incubation with 5B5T, 1EBet4B5T, 1BBet4B5T, and 1HBet4B5T from the plate count method. Confocal microscopy images of these resins after incubation (C). Real-time growth curves of *S. mutans* in the presence of different dental resins within 48 h (D). $^{*}p < 0.05$, compared with 5B5T. $^{\#}p < 0.05$, compared with 1BBet4B5T.

Remarkably, significant differences are observed among three experimental resins after 9 h of incubation, since OD values exhibit a clear decrease of bacterial density from low to high following the order of 1BBet4B5T, 1EBet4B5T, and 1HBet4B5T. These results further reveal that 1BBet4B5T has the best antibacterial activity in terms of *S. mutans* inhibition. This is mainly caused by the difference of the alkyl chain length of the comonomer, which affects the ability to penetrate, disrupt, or inhibit bacterial membranes.[44,45] As described in Table 1, the alkyl chain length of EBet, BBet, and HBet is 4 (C4), 8 (C8), and 12 (C12), respectively. Regulating the alkyl chain length to the median value (C8) could maintain an appropriate surface charge density and achieve effective contact-killing by the penetration of alkyl chain into the bacterial membrane, leading to superior antibacterial activity.[46–48] However, when the chain length further increases to 12, a decline of antibacterial activity of 1HBet4B5T is obviously found. It is possible that a longer alkyl chain could curl or bend, hindering the positively charged quaternary ammonium groups, and thereby may prevent the electrostatic interactions with *S. mutans* and decrease the antibacterial efficacy finally.[6]

3.9. Water contact angle

As seen in Fig. 7(B), 1HBet4B5T has the highest hydrophobicity among all resins. It seems that our results are inconsistent with the reported findings that the more hydrophobic the surface is, the less the bacterial adhesion is.[48] In fact, bacterial adhesion on a material surface is a complicated process. In this work, the alkyl chain length of the incorporated comonomers of resin materials seems to play an essential role in bacterial adhesion.

3.10. Bacterial morphology

The structural–morphological changes of *S. mutans* in response to dental resins were investigated with SEM and TEM (Fig. 8(A)–(H)). After coculturing with 5B5T, bacterial cells exhibit continuous smooth membranes/walls and maintain cellular integrity (Fig. 8(A) and (E)), suggesting its poor antibacterial activity. In contrast, the bacterial morphologies become wrinkled and rough and the bacterial cell structures are destroyed after exposure to three experimental resins (indicated by red arrows in Fig. 8(B)–(D)), accompanied by the obvious leakage of cytoplasmic contents (observed by red arrows in Fig. 8(F)–(H)). This resultant irreversible damage to the structures of bacterial cells is responsible for bacterial cell death finally,[34] and the reasons are as follows: (1) the integrity and permeability of cell membrane are destroyed, leading to functional disorders and metabolic disorders of the cell.[49] (2) The immune system's response might be triggered, causing inflammatory reactions and tissue damage.[50] (3) Some specific proteins or inhibition of gene expression might also be activated, further accelerating the cell death process.[51]

3.11. Protein leakage and ion-release analysis

The cytoplasm leakage observed by TEM images was quantitatively analyzed with the protein leakage and the ion release. The leakage of bacterial extracellular protein of 5B5T is 0.2 mg mL^{-1},

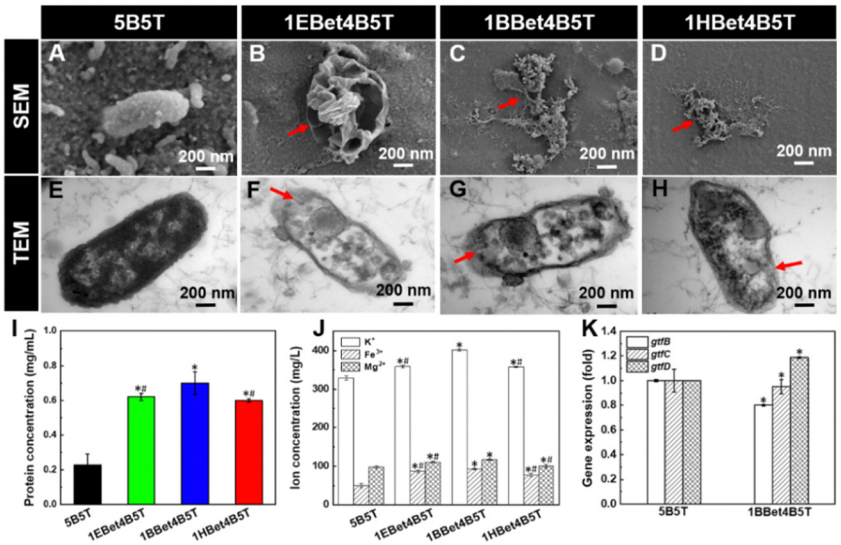

Fig. 8 SEM (A)–(D) and TEM (E)–(H) images of 5B5T (A and E), 1EBet4B5T (B and F), 1BBet4B5T (C and G), and 1HBet4B5T (D and H) after incubation with *S. mutans* for 24 h. Red arrows in images (B)–(D) and (F)–(H) indicate visible damage to the bacterial cell membranes/walls and loss of cellular integrity and the cytoplasm leakage, respectively. Protein leakage (I) and ion concentration (J) from *S. mutans* suspensions treated with 5B5T, 1EBet4B5T, 1BBet4B5T, and 1HBet4B5T for 24 h. The expression of *gtfB*, *gtfC*, and *gtfD* by *S. mutans* on 5B5T and the optimal 1BBet4B5T resin (K). $*p < 0.05$, compared with 5B5T. $^{\#}p < 0.05$, compared with 1BBet4B5T.

while 1EBet4B5T, 1BBet4B5T, and 1HBet4B5T lead to the significant increases to 0.6, 0.7, and 0.6 mg mL^{-1} (Fig. 8(I)), approximately 2.7, 3.0, and 2.6 times higher than 5B5T, respectively. The results of ICP-OES measurements of K^{+}, Fe^{3+}, and Mg^{2+} (Fig. 8(J)) demonstrate that three experimental resins induce significant increase in ionic concentrations compared with 5B5T, where 1BBet4B5T exhibits the highest K^{+} (401.9 mg L^{-1}), Fe^{3+} (93.3 mg L^{-1}), and Mg^{2+} (117.2 mg L^{-1}) contents in the cell extracellular fluid. Therefore, both protein leakage and ion concentrations increase after being exposed to experimental resins, especially for 1BBet4B5T, indicating that the incorporation of BBet causes the most serious damage to bacterial cells. The reason can be explained by that the positively charged BBet molecule with a suitable alkyl chain length (C8) captures the negatively charged bacteria, resulting in the disturbance of electric balance, the damage to cell structures, and the increased cell permeability, which ultimately causes the lysis of bacterial cells.[52,53]

3.12. Gene expression

Except for destroying the integrity of bacterial structure, the optimal 1BBet4B5T resin with the strongest antibacterial activity was selected to investigate the *gtf* gene expression of *S. mutans*. As reported previously, *S. mutans* contains *gtfB*, *gtfC*, and *gtfD*. Generally, *gtfB* forms insoluble glucans and *gtfC* produces both insoluble and soluble glucans, which are crucial for building the biofilm architecture, whereas *gtfD* synthesizes only soluble glucans, which acts as primers for *gtfB* and is related to low pH values during the formation of cariogenic plaque.[2] Reduced expression of *gtf* genes can interfere with glucan synthesis, which in turn inhibits bacteria adhesion and biofilm formation.[54,55]

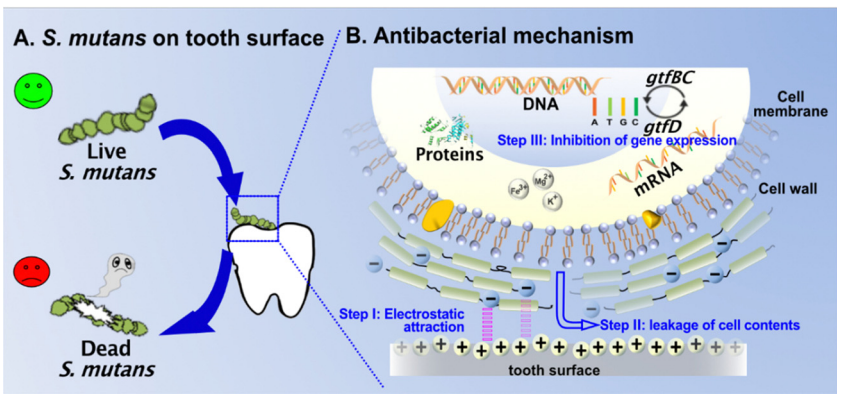

Fig. 9 Proposed antibacterial mechanism of dental resins containing Bis-QADM-Bet, including step (I) electrostatic attraction, step (II) leakage of cell contents, and step (III) inhibition of gene expression.

The significant decrease in the expression of *gtfB* and *gtfC* is found on 1BBet4B5T compared with 5B5T (Fig. 8(K)), which could be associated with the chemical structure of BBet. The presence of the cationic moiety of BBet could interact with the negatively charged exopolysaccharides of *S. mutans*, which disturbs the electric balance of the bacterial cell microenvironment and the bacterial growth, resulting in the inhibition in *gtfBC* expression.[56] Additionally, *gtfB* has extensive homology with *gtfC*, sharing approximately 75% of amino acid sequences, and both genes could be expressed coordinately.[57] Therefore, both *gtfB* and *gtfC* can be cotranscribed and subjected to the same regulatory mechanisms in the presence of 1BBet4B5T.[58] However, the *gtfD* expression is significantly increased, since *gtfD* gene located directly upstream of *gtfBC* loci is regulated in a manner opposite that of *gtfBC*.[56,59]

3.13. Antibacterial mechanism

Based on the results in Fig. 7 and 8, the contact-killing mechanism of the optimal 1BBet4B5T resin could be proposed, which involves the following three steps (Fig. 9).[60,61] (I) Electrostatic attraction: the positively charged (N^+) surface of dental resin could promote the capture of the tested bacteria with negatively charged cell wall at initial contact through electrostatic attraction. (II) Leakage of cell contents: the electric balance and the cellular integrity are disrupted due to the puncture of bacterial cell wall/membrane through the hydrophobic polymer chains (the alkyl chains). Simultaneously, the leakage of cellular ions (*i.e.*, K^+, Fe^{3+}, and Mg^{2+}) and proteins occurs. (III) Inhibition of gene expression: the expression of all targeted genes (*gtfB*, *gtfC*, and *gtfD*) of *S. mutans* is inhibited by dental resins containing Bis-QADM-Bet, which interrupts the biofilm metabolism and results in bacterial death ultimately.

4. Conclusions

In summary, three types of bis-quaternary ammonium betulin-based dimethacrylate derivatives (EBet, BBet, and HBet) were synthesized, characterized, and used as a comonomer at 10 wt% with Bis-GMA/TEGDMA based dental resins. The results showed that the performance of dental resins was strongly related to the chemical structure of EBet, BBet, and HBet. As the alkyl chain length increased to the median value (C8), the obtained BBet was clear colorless viscous liquid, endowing the resultant 1BBet4B5T resin with lower viscosity and better cell viability without scarifying its light transmittance, polymerization behavior, and mechanical properties in comparison with the control resin. More importantly, this optimal 1BBet4B5T resin significantly inhibited the growth of *S. mutans* and possessed the strongest antibacterial activity among all studied resins. This work provides a new strategy to develop dental resins with superior antibacterial activity and acceptable physicochemical properties based on the natural product betulin. Work is underway to study the *in vitro* and *in vivo* long-term antibacterial activity of these developed dental resins against more typical bacteria associated with dental caries and the related antibacterial mechanism could be further explored more accurately. In addition, the clinical application of Bis-QADM-Bet based dental materials still faces numerous challenges, such as biocompatibility and their stability in the complex oral environment. Desirable dental materials will be developed continuously towards achieving multifunctionality, high-performance, and high-selectivity.

Conflicts of interest

There are no conflicts to declare.

Acknowledgements

This work is financially supported by the National Natural Science Foundation of China (no. 51903042) and the National Key Research and Development Program of China (no. 2016YFA0201702/2016YFA0201700).

References

1 K. Cho, G. Rajan, P. Farrar, L. Prentice and B. G. Prusty, *Composites, Part B*, 2022, **230**, 109495.
2 S. L. James, D. Abate, K. H. Abate and A. Abdelalim, *Lancet*, 2018, **392**, 1789–1858.
3 B. Nijampatnam, P. Ahirwar, P. Pukkanasut, H. Womack, L. Casals, H. Zhang, X. Cai, S. M. Michalek, H. Wu and S. E. Velu, *ACS Med. Chem. Lett.*, 2021, **12**, 48–55.
4 J. W. Hofsteenge, J. D. Scholtanus, M. Özcan, I. M. Nolte, M. S. Cune and M. M. M. Gresnigt, *J. Dent.*, 2023, **130**, 104409.
5 K. R. Sims, J. P. Maceren, Y. Liu, G. R. Rocha, H. Koo and D. S. W. Benoit, *Acta Biomater.*, 2020, **115**, 418–431.
6 F. Li, M. D. Weir and H. H. K. Xu, *J. Dent. Res.*, 2013, **92**, 932–938.
7 A. Aminoroaya, R. E. Neisiany, S. N. Khorasani, P. Panahi, O. Das, H. Madry, M. Cucchiarini and S. Ramakrishna, *Composites, Part B*, 2021, **216**, 108852.
8 Y. W. Yang, Z. X. Xu, Y. Q. Guo, H. C. Zhang, Y. N. Qiu, J. X. Li, D. Y. Ma, Z. Q. Li, P. Zhen, B. Liu and Z. J. Fan, *Dent. Mater.*, 2021, **37**, 636–647.
9 A. Hoxha, D. G. Gillam, A. Agha, N. Karpukhina, A. J. Bushby and M. P. Patel, *Dent. Mater.*, 2020, **36**, 973–986.
10 L. Schnaider, M. Ghosh, D. Bychenko, I. Grigoriants, S. Ya'ari, T. S. Antsel, S. Matalon, R. Sarig, T. Brosh, R. Pilo, E. Gazit and L. Adler-Abramovich, *ACS Appl. Mater. Interfaces*, 2019, **11**, 21334–21342.
11 H. Lai, X. Peng, L. Li, D. Zhu and P. Xiao, *Prog. Polym. Sci.*, 2022, **128**, 101529.
12 E. I.-R. Kenawy, S. D. Worley and R. Broughton, *Biomacromolecules*, 2007, **8**, 1359–1384.
13 A. R. Cocco, W. L. O. Rosa, A. F. Silva, R. G. Lund and E. Piva, *Dent. Mater.*, 2015, **31**, 1345–1362.
14 X. L. He, L. Y. Ye, R. Y. He, J. W. He, S. D. Ouyang and J. Y. Zhang, *J. Mech. Behav. Biomed. Mater.*, 2022, **135**, 105487.

15 M. W. Chrószcz-Porebska, I. M. Barszczewska-Rybarek and G. Chladek, *Materials*, 2022, **15**, 5530.
16 S. Imazato, J. H. Chen, S. Ma, N. Izutani and F. Li, *Jpn. Dent. Sci. Rev.*, 2012, **48**, 115–125.
17 Y. Jiao, L. N. Niu, S. Ma, J. Li, F. R. Tay and J. H. Chen, *Prog. Polym. Sci.*, 2017, **71**, 53–90.
18 L. Cheng, M. D. Weir, K. Zhang, D. D. Arola, X. D. Zhou and H. H. K. Xu, *J. Dent.*, 2013, **41**, 345–355.
19 J. G. Liang, M. Y. Li, B. Ren, T. M. Wu, H. H. K. Xu, Y. Liu, X. Peng, G. Yang, M. D. Weir, S. Y. Zhang, L. Cheng and X. D. Zhou, *Dent. Mater.*, 2018, **34**, 400–411.
20 L. Fanfoni, E. Marsich, G. Turco, L. Breschi and M. Cadenaro, *Acta Biomater.*, 2021, **129**, 138–147.
21 P. Makvandi, R. Jamaledin, M. Jabbari, N. Nikfarjam and A. Borzacchiello, *Dent. Mater.*, 2018, **34**, 851–867.
22 Y. M. Weng, X. Guo, V. J. Chong, L. Howard, R. L. Gregory and D. Xie, *J. Biomed. Sci. Eng.*, 2011, **4**, 147–157.
23 J. M. Antonucci, D. N. Zeiger, K. Tang, S. Lin-Gibson, B. O. Fowler and N. J. Lin, *Dent. Mater.*, 2012, **28**, 219–228.
24 P. Makvandi, M. Ghaemy and M. Mohseni, *Eur. Polym. J.*, 2016, **74**, 81–90.
25 M. Laavola, R. Haavikko, M. Hamalainen, T. Leppanen, R. Nieminen, S. Alakurtti, V. M. Moreira, J. Yli-Kauhaluoma and E. Moilanen, *J. Nat. Prod.*, 2016, **79**, 274–280.
26 G. Porras, F. Chassagne, J. T. Lyles, L. Marquez, M. Dettweiler, A. M. Salam, T. Samarakoon, S. Shabih, D. R. Farrokhi and C. L. Quave, *Chem. Rev.*, 2021, **121**, 3495–3560.
27 L. S. Zhang, Z. Y. Ma, R. L. Wang and M. F. Zhu, *ACS Biomater. Sci. Eng.*, 2021, **7**, 3132–3140.
28 J. W. He, E. Soderling, L. V. J. Lassila and P. K. Vallittu, *Dent. Mater.*, 2015, **31**, 575–582.
29 H. Y. Chen, S. Q. Wei, R. L. Wang and M. F. Zhu, *ACS Biomater. Sci. Eng.*, 2021, **7**, 1428–1437.
30 Z. M. Li, H. T. Zhang, G. Xiong, J. C. Zhang, R. L. Guo, L. P. Li, H. R. Zhou, G. X. Chen, Z. Zhou and Q. F. Li, *J. Mech. Behav. Biomed. Mater.*, 2020, **103**, 103515.
31 ISO 10993-5, Biological evaluation of medical devices-Part 5: Tests for *in vitro* cytotoxicity, International Organization for Standardization, 2009.
32 ASTM E2180-18, Standard test method for determining the activity of incorporated antimicrobial agent(s) in polymeric or hydrophobic materials, American Society for Testing and Materials, 2018.
33 H. Yang, Y. L. Bi, X. R. Shang, M. Y. Wang, S. B. Linden, Y. P. Li, Y. H. Li, D. C. Nelson and H. P. Wei, *Antimicrob. Agents Chemother.*, 2016, **60**, 7436–7443.
34 R. T. Zhao, M. Lv, Y. Li, M. X. Sun, W. Kong, L. H. Wang, S. P. Song, C. H. Fan, L. L. Jia, S. F. Qiu, Y. S. Sun, H. B. Song and R. Z. Hao, *ACS Appl. Mater. Interfaces*, 2017, **9**, 15328–15341.
35 J. Y. Zhang, C. X. Chen, J. X. Chen, S. S. Zhou, Y. R. Zhao, M. L. Xu and H. Xu, *ACS Appl. Mater. Interfaces*, 2020, **12**, 27866–27875.
36 Y. Z. Wang, H. F. Hua, H. M. Liu, M. F. Zhu and X. X. Zhu, *ACS Appl. Bio Mater.*, 2020, **3**, 5300–5309.
37 A. B. Al-Odayni, R. Alfotawi, R. Khan, W. S. Saeed, A. Al-Kahtani, T. Aouak and A. Alrahlah, *Dent. Mater.*, 2019, **35**, 1532–1544.
38 T. Munhoz, Y. Fredholm, P. Rivory, S. Balvay, D. Hartmann, P. da Silva and J. M. Chenal, *Dent. Mater.*, 2017, **33**, 271–279.
39 X. L. Miao, Y. G. Li, Q. H. Zhang, M. F. Zhu and H. Z. Wang, *Mater. Sci. Eng., C*, 2012, **32**, 2115–2121.
40 J. G. Leprince, W. M. Palin, M. A. Hadis, J. Devaux and G. Leloup, *Dent. Mater.*, 2013, **29**, 139–156.
41 R. L. Wang, M. Zhu, S. Bao, F. W. Liu, X. Z. Jiang and M. F. Zhu, *J. Mater. Sci. Res.*, 2013, **2**, 12–22.
42 L. G. Lovell, J. W. Stansbury, D. C. Syrpes and C. N. Bowman, *Macromolecules*, 1999, **32**, 3913–3921.
43 E. A. Munchow, A. F. da Silva, E. Piva, C. E. C. Suarez, M. T. P. de Albuquerque, R. Pinal, R. L. Gregory, L. Breschi and M. C. Bottino, *J. Mater. Chem. B*, 2020, **8**, 10797–10811.
44 H. F. Qiu, Z. Y. Si, Y. Luo, P. P. Feng, X. J. Wu and W. J. Hou, *et al.*, *Front. Bioeng. Biotechnol.*, 2020, **8**, 910.
45 S. M. A. Soliman, M. F. Sanad and A. E. Shalan, *RSC Adv.*, 2021, **11**, 11541–11548.
46 A. P. Fugolin, A. Dobson, V. Huynh, W. Mbiya, O. Navarro, C. M. Franca, M. Logan, J. L. Merritt, J. L. Ferracane and C. S. Pfeifer, *Acta Biomater.*, 2019, **100**, 132–141.
47 P. Makvandi, R. Jamaledin, M. Jabbari, N. Nikfarjam and A. Borzacchiello, *Dent. Mater.*, 2018, **34**, 851–867.
48 H. Zhou, F. Li, M. D. Weir and H. H. K. Xu, *J. Dent.*, 2013, **41**, 1122–1131.
49 S. Hiller and P. Broz, *Nature*, 2021, **591**, 36–37.
50 Y. Y. Zhang, X. Chen, C. Gueydan and J. H. Han, *Cell Res.*, 2018, **28**, 9–21.
51 C. J. Newcomb, S. Sur, J. H. Ortony, O. S. Lee, J. B. Matson and J. Boekhoven, *et al.*, *Nat. Commun.*, 2014, **5**, 3321.
52 Y. P. Gou, M. M. Meghil, C. R. Pucci, L. Breschi, D. H. Pashley, C. W. Cutler, L. N. Niu, J. Y. Li and F. R. Tay, *Acta Biomater.*, 2018, **75**, 171–182.
53 N. Beyth, I. Yudovin-Farber, R. Bahir, A. J. Domb and E. I. Weiss, *Biomaterials*, 2006, **27**, 3995–4002.
54 F. Li, Z. G. Chai, M. N. Sun, F. Wang, S. Ma, L. Zhang, M. Fang and J. H. Chen, *J. Dent. Res.*, 2009, **88**, 372–376.
55 H. Koo, M. L. Falsetta and M. I. Klein, *J. Dent. Res.*, 2013, **92**, 1065–1073.
56 L. Huang, F. Yu, X. Sun, Y. Dong, P. T. Lin, H. H. Yu, Y. H. Xiao, Z. G. Chai, X. D. Xing and J. H. Chen, *Sci. Rep.*, 2016, **6**, 33858.
57 S. D. Goodman and Q. Gao, *Plasmid*, 2000, **43**, 85–98.
58 Q. Zhang, Q. Z. Ma, Y. Wang, H. Wu and J. Zou, *Int. J. Oral Sci.*, 2021, **13**, 1–8.
59 H. Koo, J. Seils, J. Abranches, R. A. Burne, W. H. Bowen and R. G. Quivey, *Antimicrob. Agents Chemother.*, 2006, **50**, 542–546.
60 D. B. Vieira and A. M. Carmona-Ribeiro, *J. Antimicrob. Chemother.*, 2006, **58**, 760–767.
61 Z. Y. Zhou, S. G. Zhou, X. R. Zhang, S. H. Zeng, Y. Xu and W. Y. Nie, *et al.*, *Bioconjugate Chem.*, 2023, **34**, 302–325.